NIPPON STEEL TECHNICAL REPORT No. 101 NOVEMBER 2012

Technical Review

UDC 669 . 14 . 017

Metallurgical Approaches for Product Development and Process Optimization

Manabu TAKAHASHI*
Yoshiyuki USHIGAMI
Ryuji UEMORI
Masaki MIZOGUCHI
Kazuhiro KOJIMA
Natsuko SUGIURA
Takuya HARA
Hiroyuki SHIRAHATA
Akihiro UENISHI

1. Introduction

The properties required of steel vary widely according to the usage of the steel. As described in Chapter 1, various metallurgical technologies have been developed to improve such properties as strength, rigidity, press formability, machinability, toughness, fatigue durability, corrosion resistance and hydrogen embrittlement susceptibility. Aside from the chemical composition of steel, the microstructure of steel is the most important factor in order to obtain the desired properties of steel. Research and development on appropriate controls of the microstructure of steel have been conducted to increase the strength of steel with minimum (if any) deterioration in other properties or to improve other properties with the strength kept unchanged.

Steel can be strengthened using several different microstructures (ferrite, pearlite, bainite, martensite and austenite), and solid-solution and precipitation hardening in their optimum combination. The microstructural factors that govern the properties of steel are the grain size (or the structural size as a unit of fracture, etc.), the volume fraction, strength and distribution of each type of microstructure; and the texture.

In this technical review, we discuss examples of the results of basic studies on microstructure control, which is indispensable in controlling the properties of steel.

2. Study of Various Metallurgical Phenomena to Control Microstructures

2.1 Study of recrystallization process

After cold rolling, the steel is softened by annealing. In this process, properties of the final steel product are controlled at the same time. For cold-rolled carbon steel sheet, the deep drawability of the steel sheet for press forming is improved by increasing the intensity of crystal orientation groups with {111} planes on the sheet surface (γ fibers) during annealing recrystallization (primary recrystallization). In addition, after primary recrystallization, the magnetic property of the steel sheet is controlled by secondary recrystallization whereby only grains of specific orientation are allowed to grow. Those properties are attributable to the texture of steel.

Described below are the results of our basic study on the texture forming mechanism of primary and secondary recrystallization.

2.1.1 Texture formation mechanism of recovery/recrystallization

For automotive steel sheet for deep drawing, two r-value reducing mechanisms have been proposed on the premise that solute carbon resides in the steel sheet before it is cold-rolled. Thus, 1) carbon which is an interstitial atom promotes the formation of a shear band during cold rolling, causing {110} <001> recrystallization to nucleate from the shear band [1], and 2) the solute carbon forms a complex with manganese, etc. (e.g. C-Mn dipole) during annealing and retards the recovery, thereby influencing the formation of a recrystallization texture [2]. Concerning the effect of 2), in particular, there are quite a few points which have yet to be clarified. In order to study the influence of 2) alone, we heat-treated a low carbon steel with titanium added (0.01C-0.1Ti) at 550℃ which is equivalent to the coiling temperature at which a part of solute carbon does not precipitate as TiC and segregate at the grain boundaries. **Fig. 1** shows a 3-D atomic map of carbon that segregated at the ferrite grain boundaries of a not rolled steel sheet after the above heat treatment [3]. Even when such a hot-rolled sheet is cold-rolled and annealed, neither the formation of a shear band nor the phenomenon of {110} <001> recrystallization occurs. On the other hand, it was confirmed that the recovery was noticeably later than in the case of a steel sheet whose solute carbon had been completely scavenged as TiC.

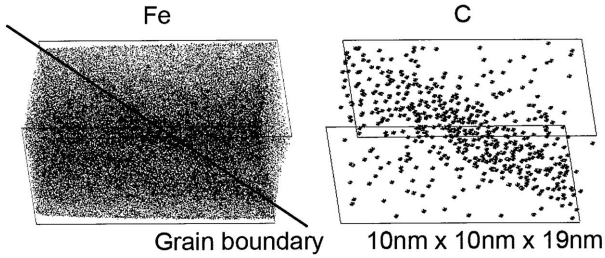

Fig. 1 3D atom map of Fe and C at a grain boundary in the hot rolled sheet annealed at 550℃

* Fellow, Ph.D., General Manager, Sheet Products Lab., Steel Research Laboratories
20-1, Shintomi, Futtsu, Chiba 293-8511

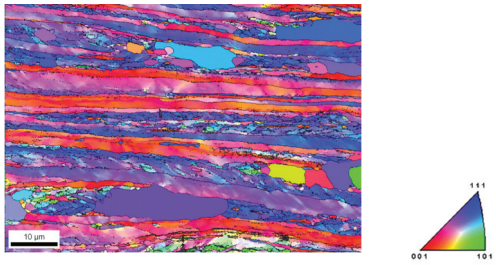

Fig. 2 ND (Normal Direction) map of the early stage of recrystallization in the steel sheet including solute carbon

Fig. 2 shows an example of an orientation map obtained by electron backscatter diffraction (EBSD) at an early stage of recrystallization. As described in a report on ordinary interstitial-free (IF) steel [4], the nucleation for recrystallization originated from {111} <112> deformed grains. However coarse recrystallized grains extending in the rolling direction encroached on neighboring deformed regions. The orientation of those recrystallized grains was mainly {111} <110>, although it was somewhat random. In the ordinary IF steel, recrystallization progresses with the growth of sub-grains, which are formed in {111} <112> deformed grains in the recovery process. Therefore, the main orientation of the nuclei becomes the same as that of the rolled grains, that is, {111} <112> [4]. In the case of a steel whose recovery is retarded by solute carbon, it is considered that the regions showing a large misorientation from the surrounding regions (mainly {111} <110>) and having a high density of dislocation, will recrystallize, and that the {111} <110> nuclei encroach on the surrounding {111} <112> region at an early stage. Thus, we consider that the delay in recovery due to the presence of solute carbon influences the recrystallization behavior and texture formation, thereby causing the r-value of steel sheet to decrease.

2.1.2 Selective growth characteristic of secondary recrystallized grains

Since the axis of easy magnetization of iron is in the <001> direction, the magnetic properties of electrical steel sheet improve when its crystal orientation is controlled properly. The degree of crystal orientation of electrical steel sheet of the highest grade available today is about 3°. A phenomenon called secondary recrystallization is utilized to control the crystal orientation.

Secondary recrystallization is the phenomenon whereby only {110} <001> grains that have good magnetic properties evolves to coarse grains of several to several tens of millimeters in size, which are thousands of times larger than the matrix grains of about ten micrometers when the steel sheet is heated at high temperature. Since secondary recrystallization is influenced by fine precipitates called inhibitor, it was difficult to make a systematic study of the phenomenon with ordinary methods of analysis. Therefore, we used synchrotron radiation, which is a powerful X-ray source, to study the mechanisms of secondary recrystallization by dynamically observing the grain growth behavior without taking the specimens out of the reheating furnace.

In order to study the behavior of selective grain growth, we prepared {110} <001> grains and {110} <115> grains (12° dispersion orientation) and carried out a dynamic observation of the growth behavior of those secondary recrystallized grains (**Fig. 3**) [5]. As a result, it was found that the {110} <001> grains begin to grow at lower temperatures than do the {110} <115> grains. Because of this difference in the onset temperature of secondary recrystallization, the selective growth of {110} <001> grains takes place in the transition temperature range of 980℃ to 1,020℃. At higher temperatures, the selective growth characteristic disappears gradually.

Comparing grain growth behavior in the above temperature regions, as shown in **Fig. 4**, the growth front for secondary recrystallized grains in the higher temperature region appears comparatively flat, whereas in the transition temperature range the growth front looks irregular and only some specific parts indicated by arrows show local grain growth. An examination of those locally

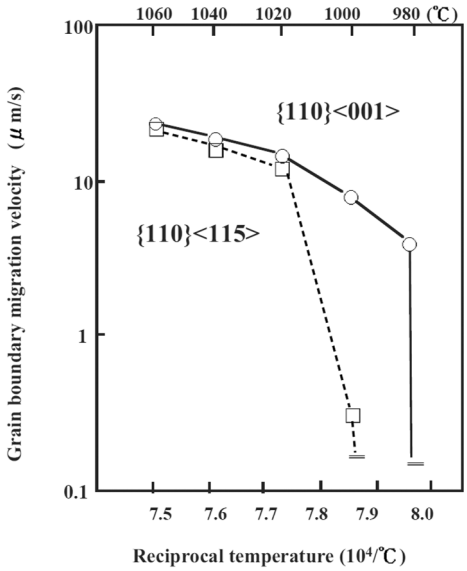

Fig. 3 Effect of temperature on the average grain growth velocity

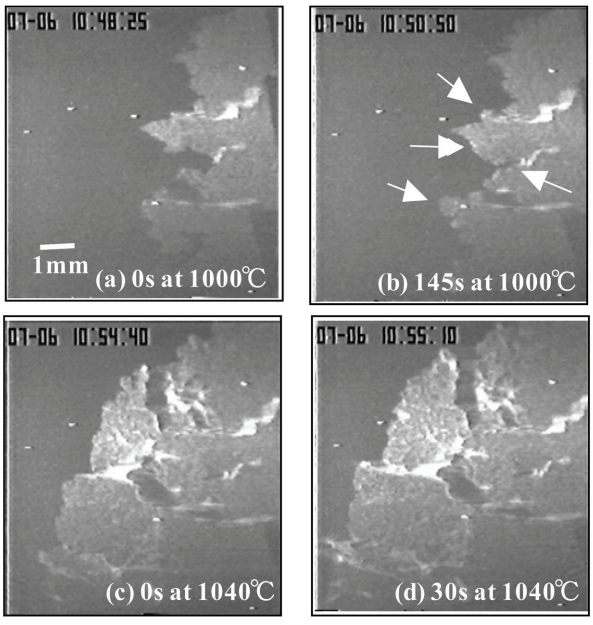

Fig. 4 X-ray topographs of {110}<001> secondary grain (a)(b): annealed at 1,000℃, (c)(d): annealed at 1,040℃

consumed matrix grains showed that the frequency of grains which have good lattice compatibility, i.e. coincidence site lattice (CSL) relationships, to {110} <001> grain is high [6].

Therefore, we concluded that secondary recrystallization is explained in terms of the selective growth mechanism with the preferential consumption of CSL grains as the elementary process.

On the basis of the above model, we formulated the phenomenon of secondary recrystallization and simulated it using a computer. As a result, it was confirmed that the grain growth behavior of coarse grains thousands of times larger than matrix grains is reproduced and that the influences of inhibitors, etc. are quantitatively evaluated [7, 8].

By taking advantage of the above understanding and computer-aided simulation of secondary recrystallization, we consider it possible to further improve the properties of electrical steel sheet.

2.2 Microstructure control by phase transformation

The balance between strength and the other mechanical properties of steels is determined by their combinations of microstructures (multiphase structure). Aside from the texture described above, the main factors here are the type, size, volume fraction and strength of the microstructures.

In view of the ever-increasing demand for stronger materials in diverse fields, it can be said that the microstructure of steels used changes from mixtures of ferrite and pearlite to mixtures of bainite and martensite. In this section, we describe the results of our study on the effect of boron (B), which is known to improve the hardenability of steel during the phase transformation, and the transition from upper to lower bainite through iron carbide precipitation behavior in bainite, which has become common to high strength steels.

2.2.1 Effect of addition of B and Nb or Mo on hardenability

It is already known that the combined addition of B and niobium (Nb) or molybdenum (Mo) significantly improves the balance between strength and toughness of steel [9-13]. In either case, even when the cooling rate is considerably slow (e.g. equivalent to air-cooling), B works effectively to increase the steel hardenability (lower the γ / α transformation temperature) and improve the steel strength markedly. We discuss below how the addition of Nb/B or Mo/B improves the mechanical properties and hardenability of steel.

Fig. 5 shows the effects of the addition of Nb-B/Mo-B on the tensile strength and low temperature toughness of a 0.015 mass% carbon steel plate (thickness: 20 mm) rolled with interrupted water-cooling (an average cooling rate in the mid-thickness between 800 and 500℃ was 20℃/s). The addition of B had minimal effect on the strength of the C-Mn steel. Instead, it caused the steel toughness to deteriorate. On the other hand, the addition of Nb-B or Mo-B improved the balance between strength and low temperature toughness much more than the addition of B alone. In particular, the effect of the addition of Nb-B was conspicuous. The microstructure of steel with B alone added consisted mainly of polygonal ferrite and contained only a small proportion of bainite. By contrast, the microstructure of the steel with Nb-B or Mo-B added consisted entirely of bainite with elongated prior γ -grain boundaries. The implication is that when the cooling rate is not as high as in direct quenching, the addition of Nb-B or Mo-B is a very effective means of significantly improving the balance between the strength and low temperature toughness of steel.

A comparison of the continuous cooling transformation diagrams of B steel, Nb-B steel and Mo-B steel after hot working shows that the γ / α transformation temperature of the Nb-B steel and Mo-B steel, respectively, was lower than that of the B steel. When the cooling rate was 60℃/s, the microstructure of each of the three steels consisted entirely of bainite. Even so, the γ / α transformation temperature of the Nb-B steel and Mo-B steel was lower than that of the B steel. **Fig. 6** shows the distribution of B in each of the B steel, Nb-B steel and Mo-B steel, observed using the α -ray track etching (ATE) method. The B steel revealed coarse precipitates of B (indicated by arrows) at prior γ-grain boundaries. (The precipitates were identified as $Fe_{23}(C,B)_6$ by electron diffraction pattern.) By contrast, the Nb-B and Mo-B steels revealed no B precipitates, suggesting that the B had segregated at the prior γ-grain boundaries. It is already known that the improvement of hardenability by addition of B is attributable to the segregation of B atoms at the prior γ -grain boundaries, but that the hardenability deteriorates markedly when coarse B precipitates are formed [9-13]. We consider, therefore, that the reason why the hardenability was improved by the addition of Nb-B or Mo-B is that the formation of B precipitates ($Fe_{23}(C,B)_6$) was restrained.

The mechanisms by which the addition of Nb-B or Mo-B improves the hardenability (lowers the γ / α transformation temperature) are not yet clearly understood. It is conceivable, however, that the addition of Nb (Mo) caused, e.g. 1) a delay in diffusion of B into γ -grain boundaries, 2) a delay in diffusion of B into B precipitates at γ -grain boundaries, or 3) a decrease in the amount of B in B precipitates (a change in the composition of B in $Fe_{23}(C,B)_6$), etc. In the future, we intend to clarify the mechanisms using a high precision analyzer, first-principles calculations and thermodynamic calculations.

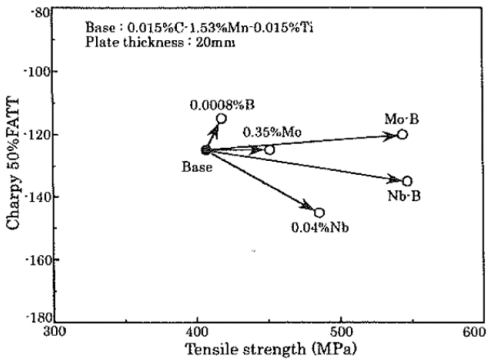

Fig. 5 Relationship between tensile strength and low temperature toughness of 0.015%C steels with interrupted water-cooled (chemical compositions are all in mass%)

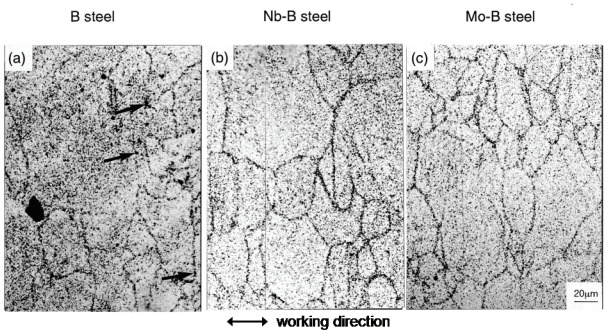

Fig. 6 α -ray track etching images of 0.015 mass% C steels with B, Nb-B and Mo-B addition (cooled at 60℃/s)

2.2.2 Modeling of bainite transformation and transition from upper to lower bainite

Generally speaking, the microstructure of steels after bainite transformation is made up of bainitic ferrite and iron carbides and can be divided into upper bainite, in which iron carbides precipitate directly from austenite, and lower bainite, in which iron carbides precipitate in bainitic ferrite. It is said that in terms of the toughness and local deformability of steels, in particular, the latter is advantageous. Here, we describe an example of our modeling of bainitic ferrite and cementite formations as competing reactions.

Bainite transformation progresses with the nucleation accompanying carbon diffusion and the growth without carbon diffusion, and the increase in volume fraction is due to the successive nucleation of sub-units whose size depends on the transformation temperature (driving force for nucleation) and austenite strength.

We applied the classical nucleation theory and assumed that the transformation starts when the driving force for nucleation of bainitic ferrite exceeded the critical driving force, G_N (= 3.637T – 1537, T: temperature), reported by Bhadeshia[14]. In order to introduce the autocatalytic effect of nucleation, we also assumed that the initial nucleation rate, Io, is accelerated by the increase in volume fraction of bainitic ferrite, $V_{\alpha B}$ [14].

$$I = (1 + \beta V_{\alpha B}) Io \qquad \beta : \text{constant} \qquad (1)$$

Bainitic ferrite is formed with the identical chemical composition as austenite, and the supersaturated carbon diffuses into the surrounding untransformed austenite.

Cementite can precipitate in carbon-supersaturated austenite and in bainitic ferrite from which carbon is being expelled. From the results of several observations, we concluded that cementite forms under paraequilibrium conditions. Therefore, we adopted the classical nucleation theory and the carbon diffusion controlled growth of disk-shaped grains. When cementite is held at the same temperature for a long time, various alloying elements contained in the cementite diffuse. However, since the ordinary heat treatment process for steel sheet is comparatively short, the effect of such diffusion was neglected. When cementite precipitates in austenite, the bainite is called upper bainite, whereas it is called lower bainite when cementite precipitates not only in austenite but also in bainitic ferrite [15]. From experimental data about bainite transformation and cementite precipitation in alloys with silicon (Si), which retards the precipitation of cementite, the parameters for interfacial energy and nucleation site density were determined [16].

Fig. 7 shows the calculated results of bainite transformation from 100% austenite at two different temperatures [16]. It can be seen that all of the cementite was formed in austenite at 450℃, whereas at 300 ℃ cementite precipitated not only in the austenite, but also in the bainitic ferrite. It is, therefore, possible to simulate the transition from upper to lower bainite by treating the cementite precipitation and the bainitic ferrite formation independently. In addition, the model allows us to accurately express the behavior of transformation at around 400℃ in a high strength steel with Si or some other elements which retard the formation of cementite. For example, it can be applied to clarify the optimum heat treatment conditions for low-alloy TRIP-type multiphase steels.

3. Control of Mechanical Properties

3.1 Relationship between toughness and microstructure of steel

As mechanical properties of steel, not only strength, ductility and toughness, but also fatigue characteristics, yield strength, high-temperature strength, and high-speed deformation characteristics, etc. may be cited. In this section, we focus on the influence on steel yield strength and toughness of M-A (martensite-austenite constituents), which are detrimental to the base metal and welds; the improvement of weld toughness by ferrite formed through intragranular transformation; and the influences of strengthening mechanisms and untransformed austenite on high speed deformation characteristics, such as the crashworthiness of automobiles.

3.1.1 Analysis of nano-scale deformation characteristics of steel containing M-A

It is already understood that M-A, which is a hard phase less than several micrometers in size and which exists in high strength steel plate, causes the steel fracture toughness and yield strength to be deteriorated. The deterioration of those mechanical properties is considered due to the stress/strain concentration that occurs because the M-A is harder than the surrounding matrix [17], and the transformation strain introduced to the matrix as a result of the increase in volume of M-A during transformation from austenite (γ) into martensite (M) [18]. Therefore, as a basic study to formulate guidelines on the control of mechanical properties of steel by M-A, we analyzed the deformation characteristics of steel materials containing M-A using the nano-indentation method.

In order to study the influence of M-A on steel toughness, we applied to a 0.1%C-0.6%Si-1.8%Mn (mass%) steel with a heat cycle simulating the following welding conditions: 1,400℃ for 1 s and cooling from 800℃ to 500℃ in 100 s. Part of the steel was also subjected to sub-zero treatment (i.e. repeated immersion in liquid nitrogen) for microscopic observation and Charpy impact testing.

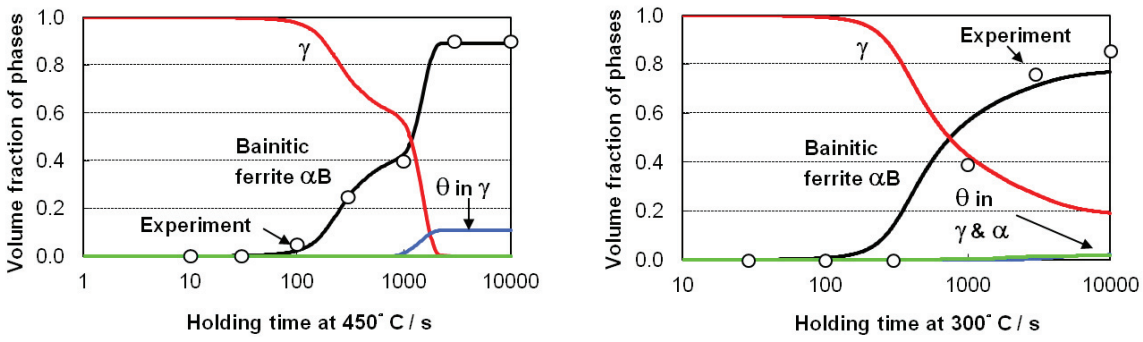

Fig. 7 Calculated change in volume fractions of bainitic ferrite, cementite and austenite in a Fe-0.6%C-1.5%Si-1.5%Mn alloy transformed at 300 (right) and 450℃ (left) (α B: bainitic ferrite, γ : austenite, θ : cementite)

Concerning the M-A, the composition was analyzed by EBSD and the hardness was measured using the nano-indentation method [19].

In the steel that was subjected to the above heat cycle, about 5% M-A was formed and the greater part of the M-A was confirmed to be γ . It was found that the γ in the M-A was transformed into M by the sub-zero treatment and that the toughness of the steel deteriorated as a result of the sub-zero treatment.

We then measured the hardness of the γ and M in the M-A using the nano-indentation method. **Fig. 8** shows examples of surface profiles and phase changes after the measurement of nano-hardness. In the scanning probe microscopy (SPM) image (a) obtained before the measurement, the "M-A" surface is flat γ . In the SPM image (b) after the measurement, the "M-A" surface looks irregular and the γ can no longer be seen. This is probably due to the transformation of γ into M as a result of the indentation. Thus, the implication is that the γ in M-A is unstable. **Fig. 9** shows the results of nano-hardness measurement. For γ , the results obtained with γ which was transformed into M and the results obtained with γ which remained untransformed are shown separately. It can be seen that the γ in the M-A is harder than α (4 to 6 GPa), but softer than M. This difference in nano-hardness is considered to account for the deterioration in steel toughness as a result of the sub-zero treatment.

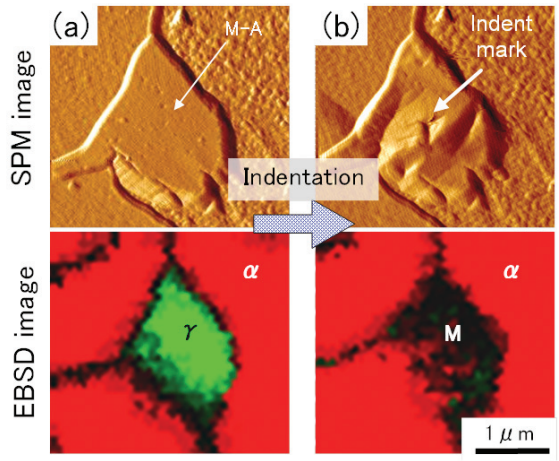

Fig. 8 Changes of scanning probe microscopy(SPM) image and EBSD phase image by nano-indentation measurement

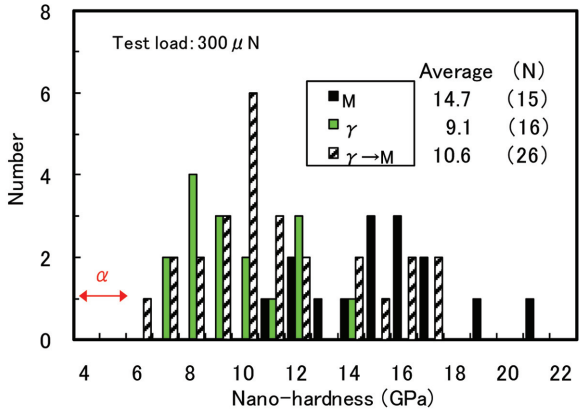

Fig. 9 Results of nano-hardness measurement

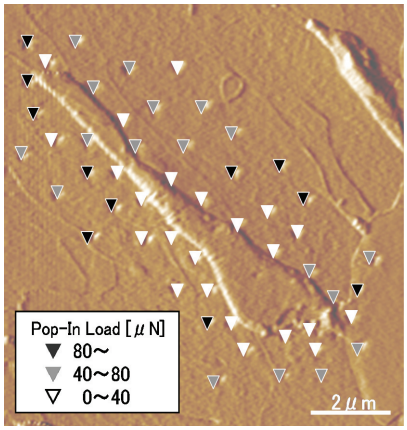

Fig. 10 Distribution of pop-in load around martensite

Next, in order to clarify the influence of M-A on steel yield strength, we applied to a 0.05%C-0.3%Si-1.5%Mn (mass%) steel the same heat cycle as mentioned above and measured the behavior of nanometer-scale deformation using the nano-indentation method in the region surrounding the M-A formed in the steel [20].

It is known that in nano-indentation testing, the pop-in phenomenon whereby the specimen shifts from elastic deformation to plastic deformation during the test occurs. When the matrix around M was indented, a decline in pop-in load was confirmed at points very close to the M as shown in **Fig. 10**. By contrast, such a decline in pop-in load was not confirmed around the γ . This decline in pop-in load is considered due to the mobile dislocation that was introduced to the matrix by a volume increase of γ during transformation of γ into M. This phenomenon directly reflects the nanometer-scale decline in yield strength of the matrix around M and is considered to account for the rounding of the stress-strain curve on a macro scale. Incidentally, a decline in pop-in load was also confirmed in the matrix around M into which γ had been transformed by indentation.

As has been described above, we could confirm that it is possible to evaluate the composition and hardness of M-A by means of EBSD and indentation and that the composition and hardness of M-A influence the toughness and yielding behavior of steel. This suggests that it should be possible to control those properties of steel materials by the thermal and dynamic stability of M-A.

3.1.2 Technology for improving HAZ toughness of high performance steel plates using intragranular transformation

The heat-affected zone (HAZ) is susceptible to deterioration in toughness since the fine microstructure imparted to the steel plates during the manufacturing process is demolished. It is well known that in order to secure the desired HAZ toughness, as well as base metal toughness, it is effective, for example, to refine the effective grain size (d_{eff}), to increase the matrix toughness of HAZ, and to reduce such hard embrittled phases as M-A from which a fracture can originate. As a means of refining the effective grain size, an intragranular ferrite (IGF) technology that utilizes nonmetallic inclusions has been put to practical use. In this subsection, we introduce the IGF technology with the focus on the manganese-depleted zone around nonmetallic inclusions that is one of the dominant mechanisms of intragranular transformation.

The mechanisms of IGF transformation have not been completely clarified yet though. The metallurgical factors that have been discussed as major ones in the IGF transformation include, for example, the steel composition, thermal history, the layer that is depleted in solute atoms (also known as the lean region) in the adjacent region of the nonmetallic inclusions/matrix interface, the elastic strain energy generated by a difference in the thermal expansion coefficient between nonmetallic inclusions and the matrix, and lattice mismatch (or interfacial energy) at interfaces between nonmetallic inclusions and the austenitic matrix and between nonmetallic inclusions and ferrite [21-23]. Given the same macroscopic conditions (i.e. same steel composition and thermal history), it has been considered that the influence of the layer depleted in solute atoms in the adjacent region of nonmetallic inclusions/matrix interfaces is especially remarkable. We show below examples of the depleted zones measured (i.e. the depleted zones around MnS, which precipitates with TiN or oxides of Ti in most cases) and describe their effects on the IGF transformation.

It has been clarified experimentally that a layer which is depleted of solute atoms influences the driving force for transformation around the nucleus formed and that any heat treatment that eliminates the depleted zone causes the driving force to disappear. For example, according to the calculated simulation results on MnS (1.0 mass% to 1.5 mass% Mn steels) [24], if there is a decrease in S concentration at the austenite/MnS interface due to the S diffusion, the "depth" of the manganese-depleted zone (maximum difference in concentration from the bulk concentration) is approximately 0.2 to 0.4 mass%. It has also been reported that when the rate of S diffusion is sufficiently high and the Mn concentration at the interface becomes equal to the bulk concentration, the concentration is around 1% and the width of the depleted zone is approximately several hundred nm. According to the measured results of manganese-depleted zones under transmission electron microscope (TEM), the depth of the depleted zone depends on the S concentration and thermal history, and the Mn concentration varies in the range 0 to 1.0 mass%. It can be said that the measured results agree well in power order with the simulated ones (**Fig. 11**) [24].

Depleted zones in TiN-MnS commercial steels (S = 0.0038 mass%) have also been studied [25-27]. **Fig. 12** shows the results of IGF area fraction measurements under different heat treatment conditions. The transformation behavior, according to this figure, differs depending to the holding temperature (at the elevated temperatures) and the holding time [25]. From the above measurement results, it can be seen that the IGF fraction varies between 0% and 80% according to the holding time and temperature, and that the IGF fraction decreases with the increase in holding time. When the holding temperature is 1,373 K, the IGF fraction decreases to only about 40% even after the steel is held for 1,000 s. At 1,523 K, however, the IGF fraction becomes almost zero in 300 s. The samples used in the above IGF fraction quantifications were then processed into thin specimens for observation under an electron microscope using the focused ion beam (FIB) method. The microstructures were observed and the decrease in Mn concentration was measured on these specimens [26-28].

Fig. 13 (a) is an SEM image revealing the presence of nonmetallic inclusions which provided an IGF nucleation site, and Fig. 13 (b) is a TEM image of the thin specimen, processed by FIB, containing that nucleation site. **Fig. 14** shows the results of composition analysis of those thin specimens (electron beam diameter: approximately 2 nm). Even after holding at 1,523 K for 1,000 seconds, the Mn concentration around nonmetallic inclusions remained the same. In other cases, the Mn concentration decreased by 0.4 and 0.2 mass% after holding at 1,373 K for 100 seconds and 1,000 seconds respectively. The decrease in Mn concentration at the interface causes the transformation temperature to rise by about 10℃ (per 0.2 mass% Mn) [29]. Therefore, it is considered to act effectively against the formation of IGF. The measured results above agree well with the calculated results for the Mn concentration distribution in austenite that accompanies the dissolution and precipitation of MnS [28]. In view of this fact and the good correspondence between the Mn concentration profile and IGF fraction shown in Fig. 12, it can be concluded that the formation of the manganese-depleted zone mentioned above plays a major role in the microstructural refinement of commercial steels.

A layer in which alloying elements are depleted around other precipitates of sulfides (CuS), carbides and nitrides is also formed. In the case of carbides and nitrides, however, the rates of C and N diffusion are extremely high even at low temperatures and hence, there is not much possibility that such depleted zones will be formed. The presence of depleted zones of such alloying elements as Nb, V and Ti has been proved by theoretical calculations as well [23], but their effects on transformation have yet to be clarified.

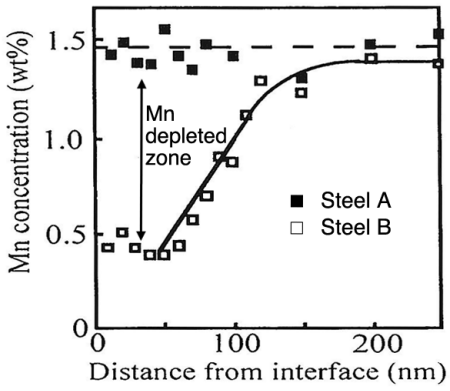

Fig. 11 Mn profiles measured by transmission electron microscopy; Steel A:0.08%C-0.0024%S-1.5%Mn Steel B: 0.10%C-0.47%S-1.5%Mn

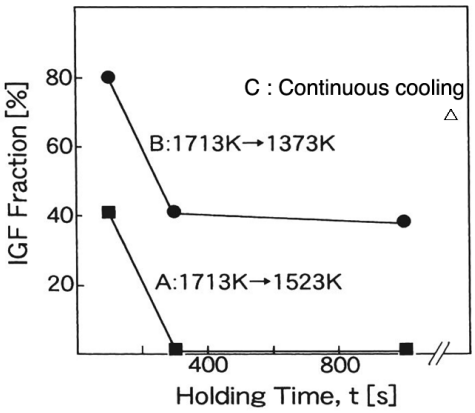

Fig. 12 Effects of holding time and annealing temperature on IGF area fraction

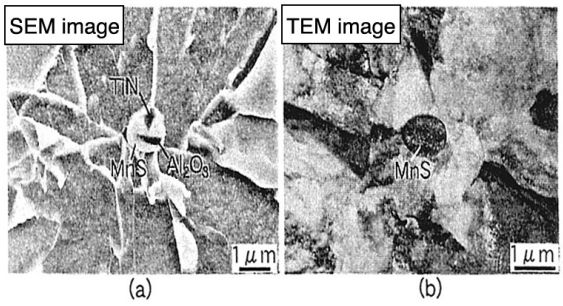

Fig. 13 Electron microscopic images of IGF nucleated on inclusion in samples annealed at 1,373K for 100s
(a) SEM and (b) TEM

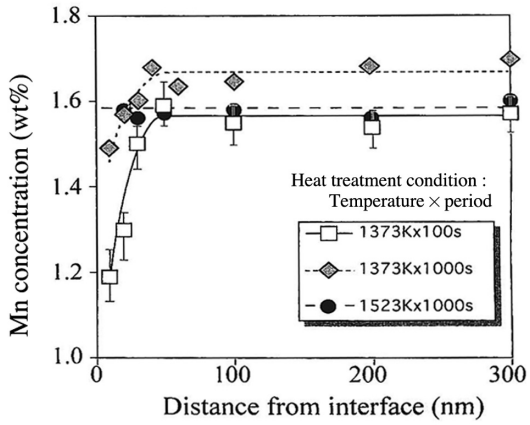

Fig. 14 Compositional profiles of Mn in steels adjacent to non-metallic inclusions (nucleation sites)

By the quantitative evaluation of element-depleted zones which have been reported on the bainite formation as well, it will become possible to control the refinement of microstructures via the utilization of intragranular transformation and to manufacture high-function and high-strength steel materials having excellent HAZ toughness.

3.2 High-strain rate deformation characteristics

It may be said that minimizing damage or injury to passengers, etc. in traffic accidents is one of the major social needs of today. In this subsection, we describe the results of our fundamental study on the response of automotive steel sheets, which could be subject to high strain rate deformation in the event of a crash.

3.2.1 Improvement in material strength and high strain rate deformation characteristics

In connection with the crashworthiness of automobiles, growing attention is being paid to the high strain rate deformation characteristics of steel—the principal material for car bodies. It is known that the flow stress of steel, which is a metal having a body-centered cubic (bcc) structure, is highly dependent on the strain rate. However, concerning high-strength steel sheets that are considered promising materials in terms of crashworthiness and being lightweight, their characteristics have not been thoroughly grasped. Since the strain rate which the automotive sheets are subjected to in a crash can reach as high as 1,000/s, or a million times the conventional strain rate, it is difficult to evaluate the actual strain rate in a crash using ordinary test equipment. That problem has been solved by the development of a high strain rate one-bar-type tensile test machine (see Fig. 2 in Chapter 1, 1-1). Using this new testing method, we studied the relationship between the strengthening of steel and the strain rate sensitivity of flow stress. The results are described below.

Various mechanisms are employed to strengthen sheet steel. Of them, solution hardening is the most fundamental and most popular. Therefore, solution-hardened materials were used as model materials, which were obtained by the addition of Mn/Si to the base material (0.002%C-0.10%Mn-0.02%Ti; mass%). Ti was added in order to remove interstitial atoms from the ferrite matrix. The materials were hot-rolled to a thickness of 2.0 mm, annealed at 700℃ for 60 minutes, and subjected to mechanical tests.

Fig. 15 shows the variation in the flow stress with the strain rate at 5% strain obtained using an ordinary tensile test machine and a high strain rate one-bar tensile test machine [30]. It was found that with all the materials, the flow stress increases with strain rate, but that the strain rate sensitivity decreases as a result of solution hardening, and there is a region in which the flow stress of the base material becomes higher than that of the Mn 1 at.% added steel. On the basis of those experimental results, we studied the deformation mechanisms by thermal activation analysis. As a result, it was found that the activation volume at high strain rates ranges from 10 to 100 b^3, which corresponds to the activation volume that is generally ascribed to the Peierls-Nabarro mechanism. Thus, it can be concluded that the rate-controlling process for the tested materials at high strain rates is the nucleation and propagation of kinks against the Peierls-Nabarro barrier, as already assumed by other authors [31]. Finally, we can discuss the decrease of strain rate sensitivity of the flow stress of solution-hardened steels as follows.

In the first place, solid solution hardening is the phenomenon whereby the flow stress at quasi-static strain rates is increased by misfit strains in the matrix (ferrite matrix) introduced by solute atoms. On the other hand, at high strain rates, the flow stress increases as overcoming the Peierls-Nabarro barrier, which has origins in the crystalline structure, becomes difficult. The smaller the disturbance in the crystalline structure (~ misfit strains), the larger becomes the increase of the flow stress at high strain rates. As mentioned above, the solute atoms introduce misfit strains in the ferrite matrix. Misfit strains facilitate the nucleation and propagation of kinks. As a result, the flow stress of the solution-hardened steels shows lower strain

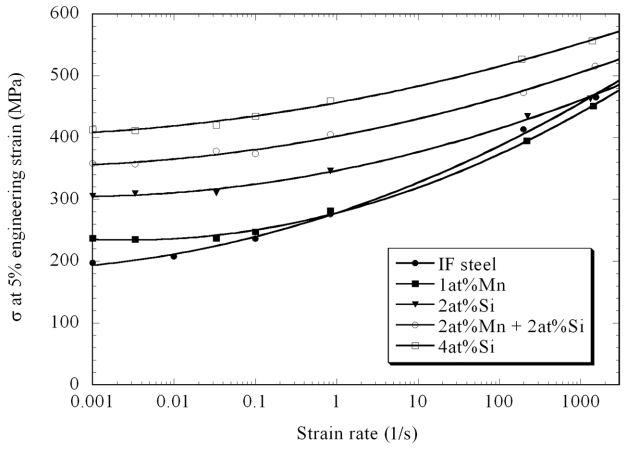

Fig. 15 Strain rate sensitivity of flow stress of solution hardened steels

rate sensitivity than that of the host steel. In this context, we can understand the results shown in Fig. 15, which shows the correlation between solid solution hardening at low strain rates and the decrease in the strain rate sensitivity at high strain rates.

We have so far extensively discussed the mechanisms of strain rate sensitivity of the flow stress in solution-hardened steels. We have also studied other types of steels that have different strengthening mechanisms. The results indicate that strengthening the matrix (ferrite matrix) always causes the strain rate sensitivity of the flow stress to deteriorate and that the degree of the deterioration is proportional to the degree of the strengthening of the ferrite matrix [32]. On the other hand, concerning TRIP steel and dual-phase (DP) steel which use the second phase for hardening, it is known that they show superior strain rate sensitivity of flow stress compared to other steels of the same strength level [33]. The strengthening of these steels is accomplished by hard (or multiple) phases, which means that the strengthening of the ferrite matrix is less than that of other steels. It can be said that this makes the strain rate sensitivity of the flow stress of these steels superior to other steels. On the basis of this understanding, it becomes possible to select an optimum steel material for the particular application.

3.2.2 Strain rate dependence of flow stress in TRIP-type multiphase steel sheets

In this subsection, we describe the high-speed deformation characteristics of practical high-strength steel sheets for automotive applications. As explained in Chapter 1, 1-1, steel sheets for any automotive parts that undergo plastic deformation to absorb crash energy are required to have good press formability and strong strain rate dependence of flow stress. One of the typical multiphase steels which meets those requirements is the low-alloy TRIP-type multiphase steel ("low-alloy TRIP steel").

In order to prevent the austenite from transforming completely in low-alloy steel with limited amounts of Ni and Mn, it is necessary to increase the C and N concentrations locally in untransformed austenite. In the case of low-alloy TRIP steel, it is required to increase the C concentration in the untransformed austenite to approximately 1 mass% for the austenite to remain untransformed at room temperature. Here, the important metallurgical points are: the To concept in the bainite transformation (To is the temperature at which austenite and ferrite of the same composition have the same free energy) and the retardation of cementite precipitation caused by the addition of Si and Al [34]. The To concept corresponds to the mechanism of diffusionless bainite transformation. Namely, the maximum possible carbon concentration attainable in the untransformed austenite is determined by the bainite transformation temperature.

For the purposes of our study, we called deformations at strain rates corresponding to those in a crash, which can be as high as 1,000/s, as "the dynamic" and the deformation at ordinary strain rates used for the conventional tensile test as "the static". In addition, we define the difference in flow stresses between dynamic and static tensile tests as the strain rate dependence ("static-dynamic difference of flow stresses"). Then, we studied the effects of bake hardening and residual austenite stability on the average static-dynamic difference at strains between five and ten percent at which the main part of the absorption of crush energy of a square tube is attained.

As mentioned above, the static-dynamic difference decreases with the increase in steel strength. On the other hand, it has been confirmed that when pre-strained steel is subjected to bake hardening (180℃, 20 min), the dynamic stress increases almost in proportion to the static stress [35]. Generally speaking, automotive parts which are made from multiphase steels having large bake-hardenability are capable of absorbing a considerable amount of impact energy [33].

In the case of low-alloy TRIP steels, the stability of residual austenite influences their high-speed deformation characteristic. It has been reported that the uniform elongation (u-El) of low-alloy TRIP steel is proportional to the product of the volume fraction of residual austenite and the cube of the carbon concentration in the residual austenite [34]. Looking at the static-dynamic difference of low-alloy TRIP steels with almost the same strength, it can be seen that the static-dynamic difference increases in proportion to the u-El (the product of the volume fraction of residual austenite and the cube of the carbon concentration of residual austenite) as shown in **Fig. 16** [34]. Thus, it can be said that stabilizing the residual austenite increases the static-dynamic difference.

We consider that the above increase in static-dynamic difference is dependent on the behavior of deformation-induced transformation of residual austenite into martensite. **Fig. 17** shows the transformation behavior of residual austenite when the strain rate was increased from 0.001/s to 10/s [34]. It can be seen that the increase in deformation promotes the transformation of residual austenite. The more stable the residual austenite is, the wider the stain region becomes in which

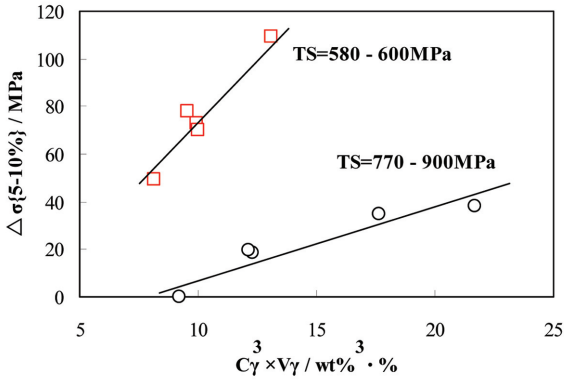

Fig. 16 Relationships between the stability of retained austenite (corresponds to u-El) and the average static-dynamic difference of flow stress between 5 and 10% of strain
(C γ : carbon concentration in retained austenite in mass%, V γ : volume fraction of retained austenite)

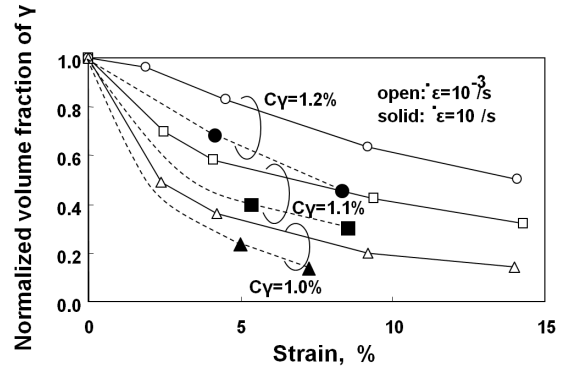

Fig. 17 Effect of strain and strain rate on the transformation from retained austenite to martensite
(C γ : carbon concentration in retained austenite in mass%, ε : strain rate in 1/s)

the rise in stress is due to deformation-induced transformation. Thus, stabilizing residual austenite, as well as increasing the amount thereof, increases the static-dynamic difference of flow stress, especially in the small-strain region [34].

4. Weld Metal with Enhanced Strength and Toughness

From the standpoint of ensuring the safety of a steel structure, the quality of its welded joints is extremely important. The toughness of a metallic material has much to do with its microstructure. It is generally said that the finer the microstructure, the greater its toughness. As an example of knowledge obtained by research on the refinement of weld metal microstructure, intragranular transformation technology utilizing micro-inclusions as the nuclei can be cited [36-38]. Unlike rolled steel materials, weld metals do no permit adding a strain in the γ phase, or implementing accelerated cooling by water, etc. It is intragranular transformation technology that effectively controls the phase transformation from γ to α. An example of intragranular transformation is shown in **Fig. 18** [36]. Radial planar structures have been formed with an oxide of Ti as the nucleus and grain boundaries having a large inclination can be seen. Since acicular ferrite, which is formed as a result of intragranular transformation, is a structure with a large inclination, it has the effect of reducing the unit of fracture surface in fracture propagation and thereby affords a weld metal with greater toughness [36]. The mechanism of intragranular transformation of weld metal is often explained in terms of misfit values [39], and it is said that the intragranular ferrite grows from TiO, TiN, galaxite, etc. which are fairly compatible with ferrite [39]. On the other hand, there is a report that the solute-depleted zone around inclusions, which has been confirmed in the heat affected zone [40], does not occur in the weld metal [41]. Thus, details of the mechanism of intragranular transformation have yet to be clarified. Industrially, weld metals whose microstructure has been controlled by intragranular transformation are widely used on a stable basis. For example, with steel materials in the HT 490-MPa class, a high toughness weld metal whose Charpy absorbed energy at −70℃ exceeds 100 J is formed even in submerged arc welding with a heat input as large as 10 kJ/mm [42]. As an example of welding a steel material with greater strength, refer to submerged arc welding of seams of X120 class UOE pipes. In this case, the microstructure of the weld metal is a fine one consisting mainly of degenerate upper bainite (DUB) [43]. It is generally said that the desired toughness of upper bainite is difficult to secure. In this particular example, however, a high-toughness weld metal whose Charpy absorbed energy at −30℃ is greater than 100 J has been obtained [44]. This may be attributable to the refinement of DUB block size by ferrite formed as a result of intragranular transformation around oxides [45], or to the influence of residual austenite film between DUB bainite laths.

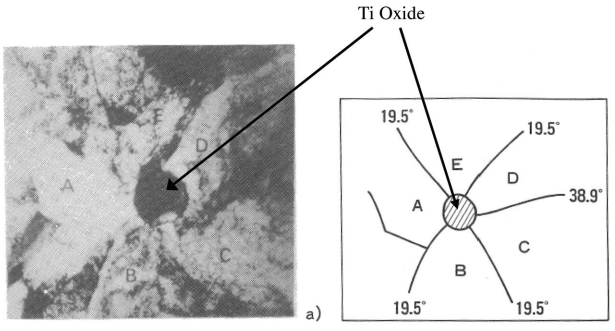

Fig. 18 TEM micrograph of intragranular ferrite nucleated on Ti-oxide particle

5. Conclusion

One of the most important methodologies of controlling the properties of steels is to control the microstructure of the steels. In order to obtain the steel properties required of the final use of the steels, it is indispensable to understand the individual processes of the microstructural development in steel production processes such as heating, working and cooling, and to predict quantitatively the microstructural development in those individual processes. Such basic understanding will lead directly to the development of high-performance steels that contribute to our environmental and social consciousness. It is also noted that this approach will enable the optimization of processing conditions for steels resulting in energy saving and a reduction in CO_2 emissions in the steel manufacturing processes.

References

1) Ushioda, K., Abe, M.: Tetsu-to-Hagané. 70, 96 (1984)
2) Hutchinson, W.B., Ushioda, K.: Scand. J. Metall. 3, 269 (1984)
3) Sugiura, N., Yoshinaga, N., Kawasaki, K., Yamaguchi, Y., Takahashi, J., Yamada, T.: Tetsu-to-Hagané. 94, 179 (2008)
4) Van Derschueren, D., Yoshinaga, N., Koyama, K.: ISIJ Int. 35, 1046 (1996)
5) Ushigami, Y., Kawasaki, K., Nakayama, T., Suga, Y., Harase, J., Takahashi, N.: Mater. Sci. Forum. 157-162, 1081 (1994)
6) Ushigami, Y., Kumano, T., Haratani, T., Nakamura, S., Takebayashi, S., Kubota, T.: Mater. Sci. Forum. 467-470, 853 (2004)
7) Ushigami, Y., Nakayama, T., Arai, S., Kubota, T.: Proc. Soft Mag. Mater. 16, 487 (2003)
8) Ushigami, Y.: Recrystallization/Texture and Its Application to Control of Microstructure. Iron and Steel Institute of Japan, 1999, p. 245
9) Iron and Steel Institute of Japan: Influence of Boron on Microstructure and Properties of Steel Materials. 1999
10) Tamehiro, H., Murata, M., Habu, R., Nagumo, N.: Trans. ISIJ. 27, 120 (1987)
11) Tamehiro, H., Murata, M., Habu, R., Nagumo, N.: Trans. ISIJ. 27, 130 (1987)
12) Asahi, H.: ISIJ International. 42 (10), 1150 (2002)
13) Hara, T., Asahi, H., Uemori, R., Tamehiro, H.: ISIJ International. 44 (8), 1431 (2004)
14) Bhadeshia, H.K.D.H.: Acta Metall. 29, 1117 (1981)
15) Takahashi, M., Bhadeshia, H.K.D.H.: Materials Science and Technology. 6, 592-603 (1990)
16) Azuma, M., Fujita, N., Takahashi, M., Iung, T.: Materials Science Forum. 426-432, 1405-1412 (2003)
17) For example, Haze, T. et al.: Seitetsu Kenkyu. (326), 36 (1987)
18) For example, Morikawa, H. et al.: Tetsu-to-Hagané. 64, S740 (1978)
19) Shirahata, H. et al.: CAMP-ISIJ. 21, 504 (2008)
20) Mizoguchi, M. et al.: CAMP-ISIJ. 21, 505 (2008)
21) Mabuchi, H., Aihara, S.: Materia. 34, 301 (1995)
22) Ohashi, T., Tamehiro, H., Takahashi, M.: Materia. 36, 159 (1997)
23) Iron and Steel Institute of Japan (ISIJ): Present Conditions of Control of Steel Microstructures and Qualities by Nonmetallic Inclusions and Study of Control Mechanisms. ISIJ Society for Basic Study, Sectional Society for Control of Steel Microstructures and Qualities Utilizing Inclusions in Steel (Chairman: Enomoto, M.), 1995
24) Shigesato, G., Sugiyama, M., Uemori, R., Terada, Y.: CAMP-ISIJ. 12, 534 (1999)
25) Aihara, S., Uemori, R., Furuya, H., Tomita, Y., Shigesato, G.: CAMP-ISIJ. 12, 1293 (1999)
26) Shigesato, G., Sugiyama, M., Aihara, S., Uemori, R., Furuya, H.: CAMP-ISIJ. 12, 1294 (1999)
27) Shigesato, G., Sugiyama, M., Aihara, S., Uemori, R., Tomita, Y.: Tetsu-to-Hagané. 87, 93 (2001)
28) Aihara, S., Shigesato, G., Sugiyama, M., Uemori, R.: Nippon Steel Technical Report. (91), 43 (2005)
29) Enomoto, M.: Metall. Trans. A25, 1947 (1994)
30) Uenishi, A., Teodosiu, C.: Acta Mater. 51, 4437 (2003)

31) Harding, J.: Acta Met. 17, 949 (1969)
32) Uenishi, A., Yoshida, H.: Journal of the Japan Society for Technology of Plasticity. 46, 646 (2005)
33) Takahashi, M., Uenishi, A., Kuriyama, Y.: Proc. of IBEC, Auto Body Materials. 1997, p. 26
34) Takahashi, M., Yoshida, H., Hiwatashi, S.: Proc. Int. Conf. on TRIP-Aided High Strength Ferrous Alloys, GRIPS' Sparkling World of Steel. Belgium, 2002, p. 103
35) Takahashi, M., Uenishi, A., Yoshida, H., Kuriyama, Y.: Proc. of IBEC, Auto Body Materials. SAE Paper Number 2003-01-2765
36) Ohkita, S., Homma, H., Tsushima, S., Mori, N.: Australian Welding J. 29 (3), 29 (1984)
37) Horii, Y., Ichikawa, K., Ohkita, S., Funaki, S., Yurioka, N.: Quarterly Journal of the Japan Welding Society. 13 (4), 500 (1995)
38) Mori, N., Homma, H., Ohkita, S., Wakabayashi, M.: Journal of the Japan Welding Society. 50 (2), 174 (1981)
39) Horii, Y.: Structure and Toughness of Welds. ISIJ Nishiyama Memorial Lecture. 1989, P. 39
40) Yamamoto, K., Hasegawa, T., Takamura, J.: Tetsu-to-Hagané. 79 (10), 1169 (1993)
41) Yamada, T., Terasaki, H., Komizo, Y.: Quarterly Journal of the Japan Welding Society. 25 (3), 416 (2007)
42) Kojima, K., Ohkita, S., Aihara, S., Imai, S., Motomatsu, R., Umeki, M., Miura, T.: Proc. 18th Int. Conf. OMAE. Newfoundland, 1999, ASME
43) Asahi, H., Hara, T., Sugiyama, M., Maruyama, M., Terada, Y., Tamehiro, H., Koyama, K., Ohkita, S., Morimoto, H., Tomioka, K., Doi, N., Murata, M., Ayukawa, N., Akasaki, H., Fairchild, D.P., Macia, M.L., Petersen, C.W., Koo, J.Y., Bangaru, N.V., Luton, M.J.: Proceedings of the 13th International Offshore and Polar Engineering Conference. Honolulu, Hawaii, USA, 2003, ISOPE
44) Morimoto, H., Shinada, T., Koyama, K., Asahi, H., Sugiyama, M., Terada, Y., Hara, T., Ayukawa, N., Doi, N., Miyazaki, H., Yoshida, T., Terasawa, T., Murata, M.: Book of Abstracts of International Conference on Pipeline Technology. 2009, p. 149
45) Ohkita, S.: Structures and Characteristics of Recent Steel Plate Welds. ISIJ Nishiyama Memorial Lecture. 2005, p. 123

Manabu TAKAHASHI
Fellow, Ph.D.
General Manager, Sheet Products Lab.
Steel Research Laboratories
20-1, Shintomi, Futtsu, Chiba 293-8511

Natsuko SUGIURA
Senior Researcher, Dr.Eng.
Kimitsu R&D Lab.

Yoshiyuki USHIGAMI
Chief Researcher, Dr.Eng.
Yawata R&D Lab.

Takuya HARA
Chief Researcher, Dr.Eng.
Kimitsu R&D Lab.

Ryuji UEMORI
General Manager, Dr.Eng.
Plate, Pipe, Tube & Shape Research Lab.
Steel Research Laboratories

Hiroyuki SHIRAHATA
Senior Researcher
Plate, Pipe, Tube & Shape Research Lab.
Steel Research Laboratories

Masaki MIZOGUCHI
Researcher
Plate, Pipe, Tube & Shape Research Lab.
Steel Research Laboratories

Akihiro UENISHI
Senior Researcher, Dr.
Forming Technologies R&D Center
Steel Research Laboratories

Kazuhiro KOJIMA
Senior Researcher
Welding & Joining Research Center
Steel Research Laboratories